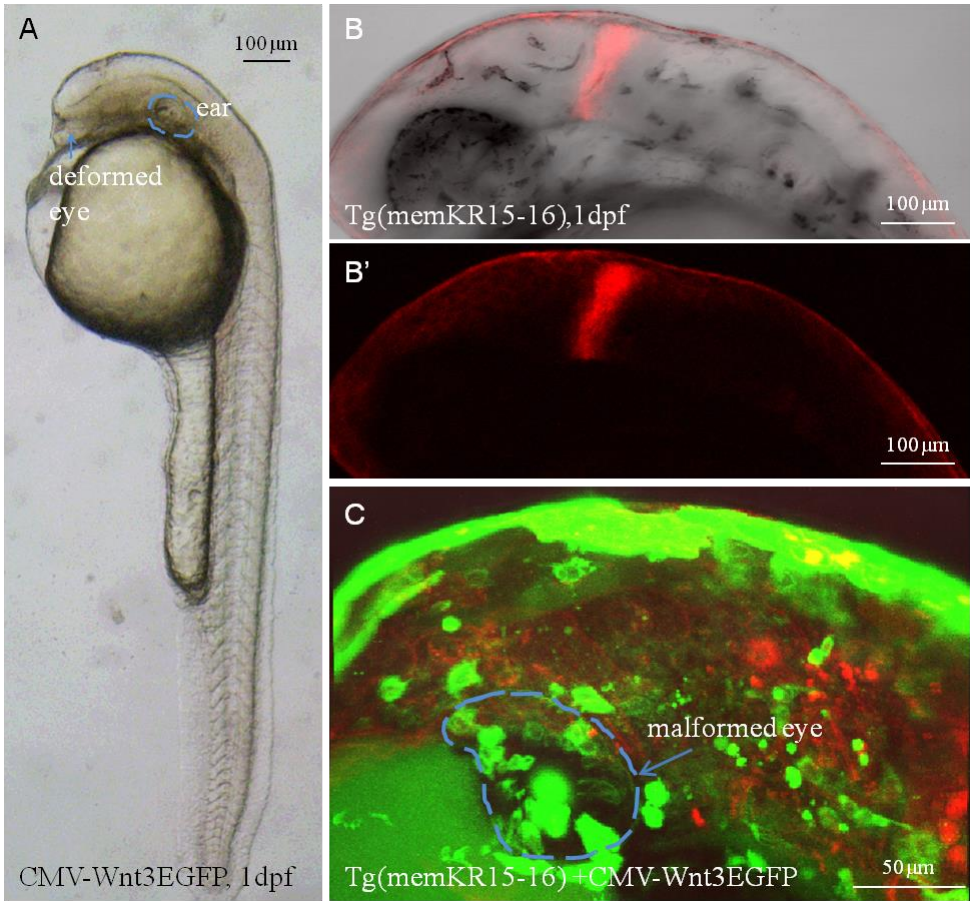


**Fig. S1. Functional overexpression of recombinant Wnt3.** The recombinant Wnt3 zebrafish fusion protein with EGFP at the C-terminal (Wnt3EGFP) is functional as overexpression in zebrafish produces a posteriorized brain phenotype typical of overt Wnt activity. (**A**) Bright field image of a malformed embryo with a posteriorized brain upon overt Wnt3EGFP expression under the ubiquitous CMV promoter. Injection of the Wnt3EGFP expression construct at blastula stage resulted in the deformed phenotype. (**B**) Tg(memKR15-16) expressed membrane localized KillerRed in the midbrain hindbrain boundary (mhb) was used to characterize the deformed brain phenotype. (**C**) The posteriorized brain phenotype is accompanied by the loss of the midbrain hindbrain boundary observed in Tg(memKR15-16) upon overt Wnt3EGFP expression.

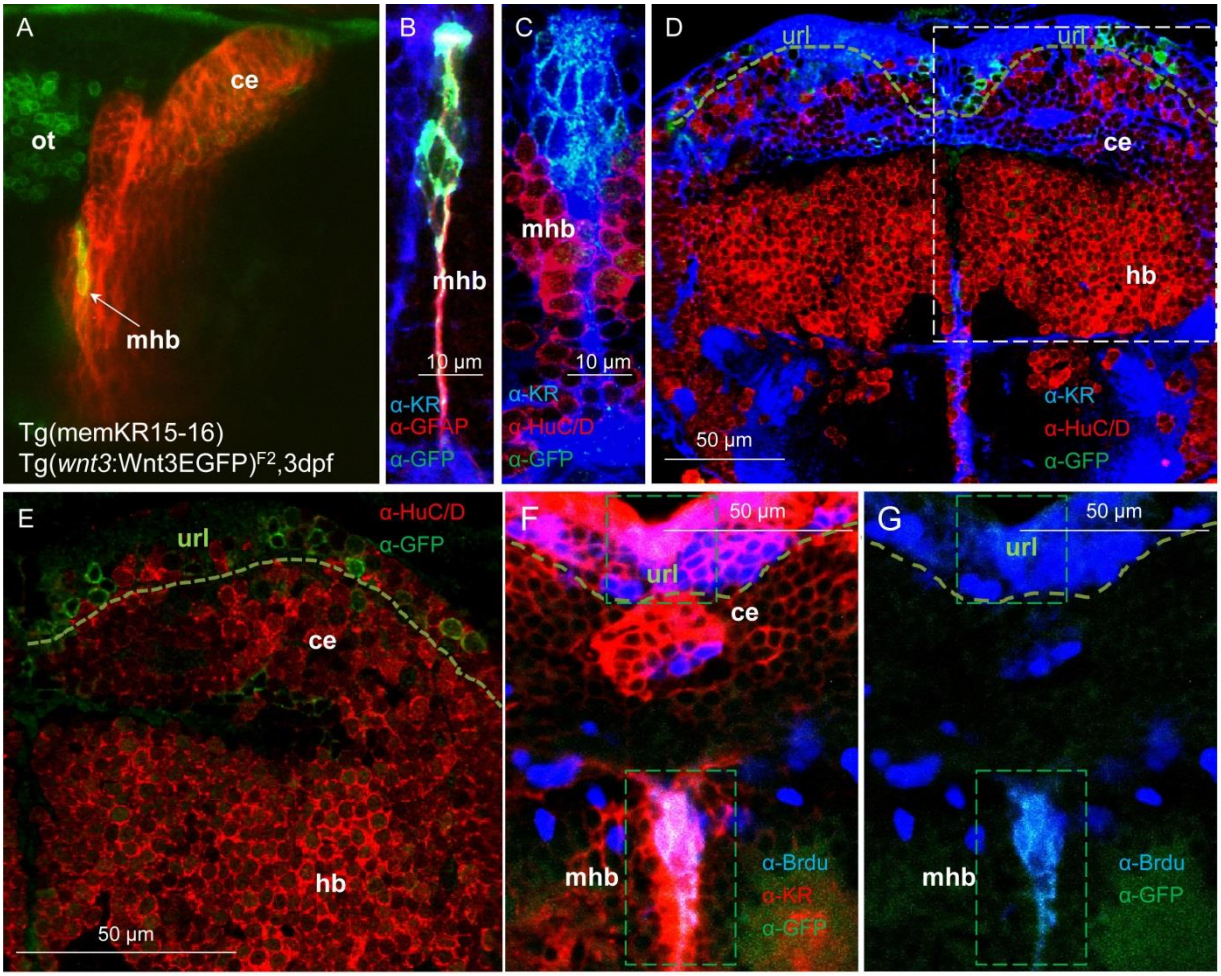


**Fig. S2. Cells expressing Wnt3EGFP in the midbrain hindbrain boundary and cerebellum are located in proliferation niches.** (**A**) An in vivo image of a double transgenic larvae co-expressing the membrane localized KillerRed in the midbrain hindbrain boundary (mhb) and cerebellum of Tg(memKR15-16) and C terminal EGFP Wnt3 fusion proteins from Tg(*wnt3*:Wnt3EGFP)$^{F2}$. Double transgenic larvae confirmed Wnt3EGFP expression in the mhb and the cerebellum. *wnt3*:*Wnt3EGFP*+ cells in the cerebellum are predominantly localized to the upper rhombic lip (url). (**B-E**)Wnt3EGFP cells at midbrain hindbrain boundary (mhb) are glial cells (**B**) as it stained positively for GFAP (glial fibrilary acidic protein) and are negative for the neuronal marker HuC/D (**C-E**). (**F-G**) Midline restricted Wnt3EGFP cells at midbrain hindbrain boundary (demarcated by membrane KR expression in this domain) are proliferating cells since they stained positively for Brdu.

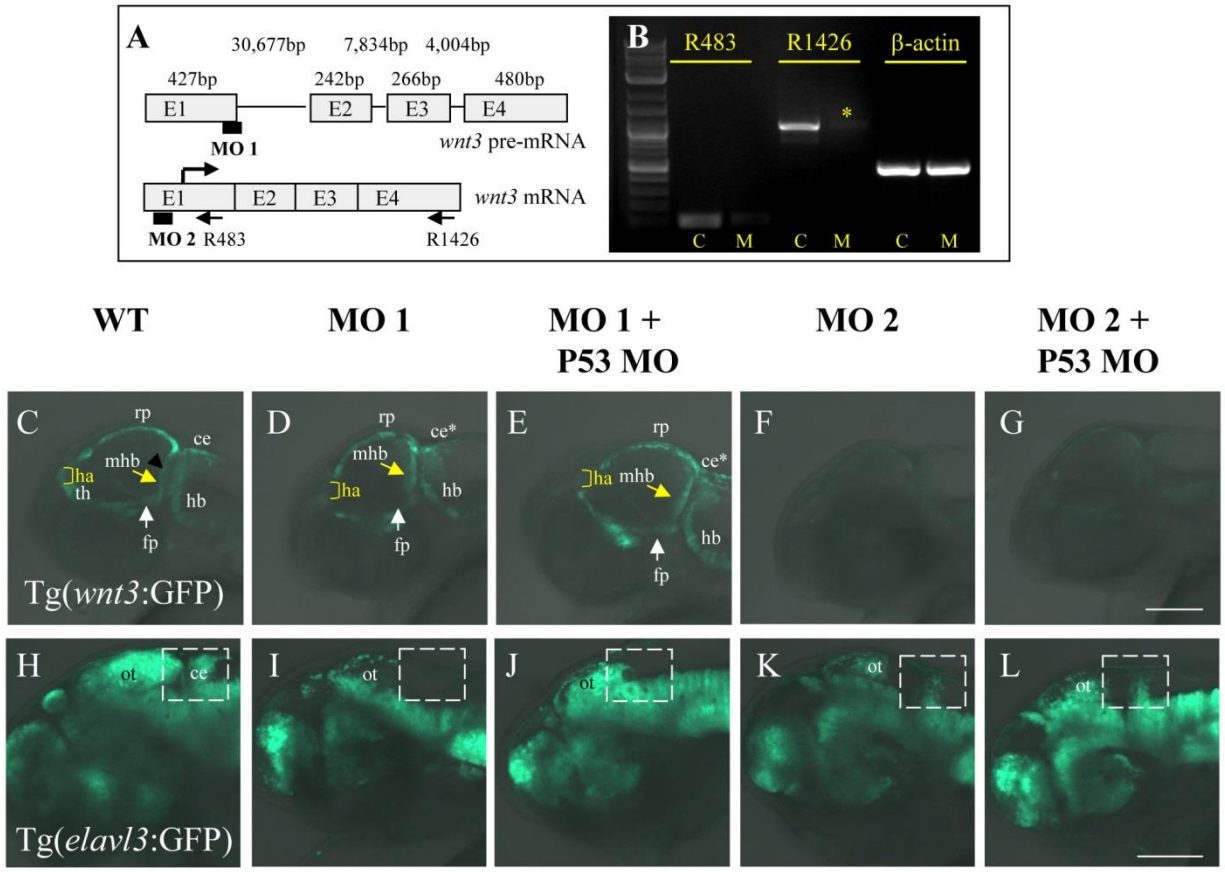


**Fig. S3. Interference with Wnt3 function disrupts cerebellar differentiation.**

(A) Organization of the *wnt3* pre-mRNA and regions targeted by *wnt3* MOs, MO 1 (targets *wnt3* exon1-intron 1 boundary) and MO 2 (targets *wnt3* 5'UTR). The length of each exon and intervening intron is indicated. (B) RT-PCR analysis of *wnt3* in wild type and morphants (MO1) at 30 hpf. Wnt3 knockdown upon microinjection of MO1 interfere with formation of wild type *wnt3* transcripts highlighted by (*). Abbreviation: control (C); MO1 injected morphants (M). (C-G) Only microinjection of translation blocking MO (MO2) whose recognition site is present in the *wnt3* regulatory element successfully interferes with GFP expression in Tg(*wnt3*:EGFP)$^{F1}$. (H-L) Wnt3 deficiency through either microinjection of MO1 or MO2 with or without p53 MO consistently reduces GFP-positive neurons in the cerebellum (ce) of 72hpf Tg(*elav*:GFP) embryos. Insert scale bar is 50 µm.

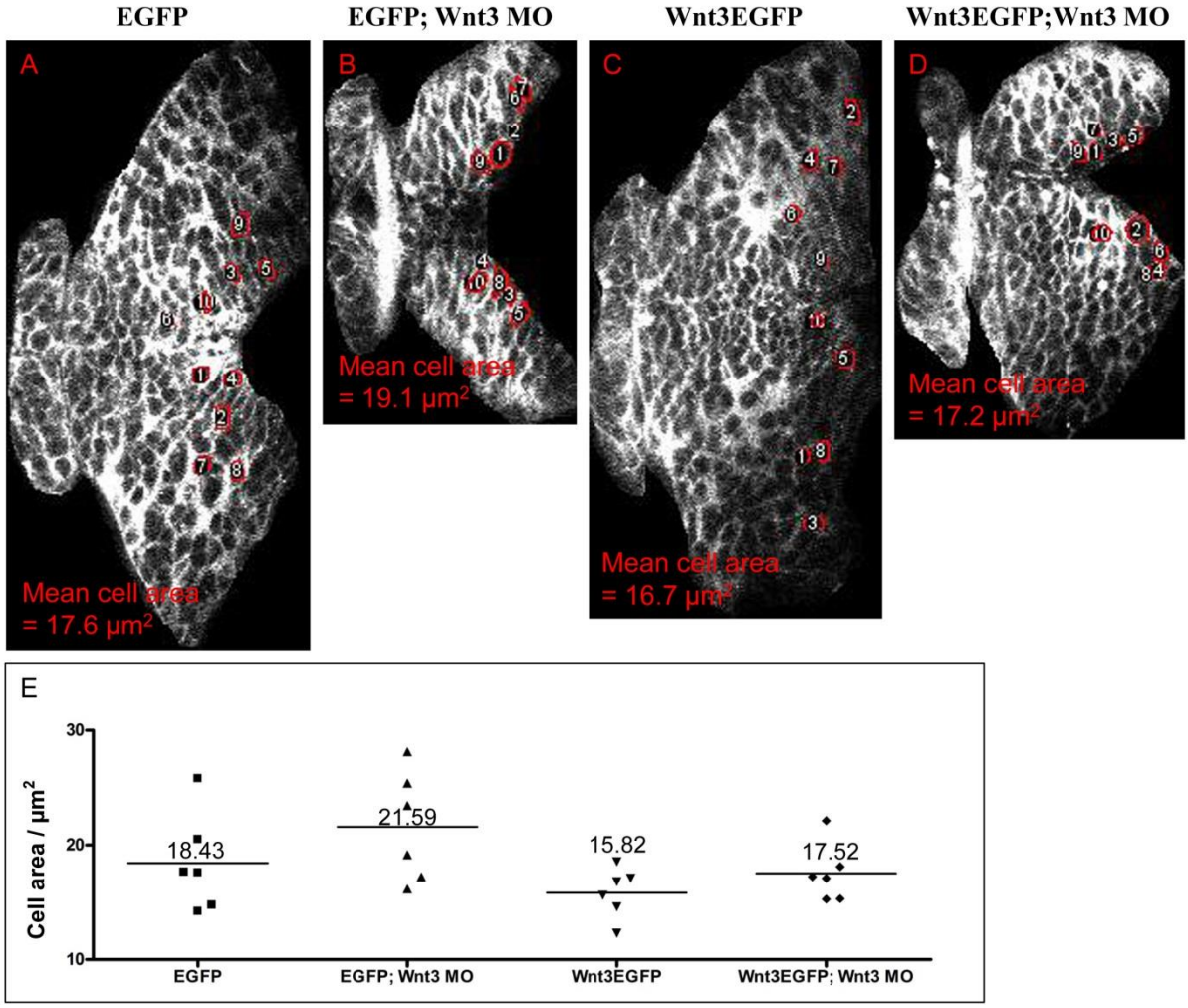


**Fig. S4. Increase in cell numbers and not cell size results from Wnt3EGFP mediated growth in the cerebellum. (**A-D) Dorsal view of KillerRed expression in the midbrain hindbrain boundary (mhb) and cerebellum of double transgenic larvae co-expressing either EGFP from Tg(wnt3:EGFP)$^{F1}$ (A-B) or Wnt3EGFP from Tg(wnt3:Wnt3EGFP)$^{F3}$ (C-D) and Tg(memKR15-16). Reduction in memKR-positive cerebellum growth is partially compensated in MO1 injected 3dpf Tg(wnt3:Wnt3EGFP)$^{F3}$(D). (E) Scatter plot of 10 mean cell area in the cerebellum, 6 samples per group, cannot detect statistically significant difference in quantified cell area. Unpaired t test comparing Tg(wnt3:EGFP)$^{F1}$ versus MO1 injected Tg(wnt3:EGFP)$^{F1}$ gives P=0.2554; Tg(wnt3:wnt3EGFP)$^{F3}$ versus MO1 injected Tg(wnt3:wnt3EGFP)$^{F3}$ gives P=0.2407. Unpaired t test comparing MO1 injected Tg(wnt3:EGFP)$^{F1}$ versus MO1 injected Tg(wnt3:wnt3EGFP)$^{F3}$ gives P=0.0957.

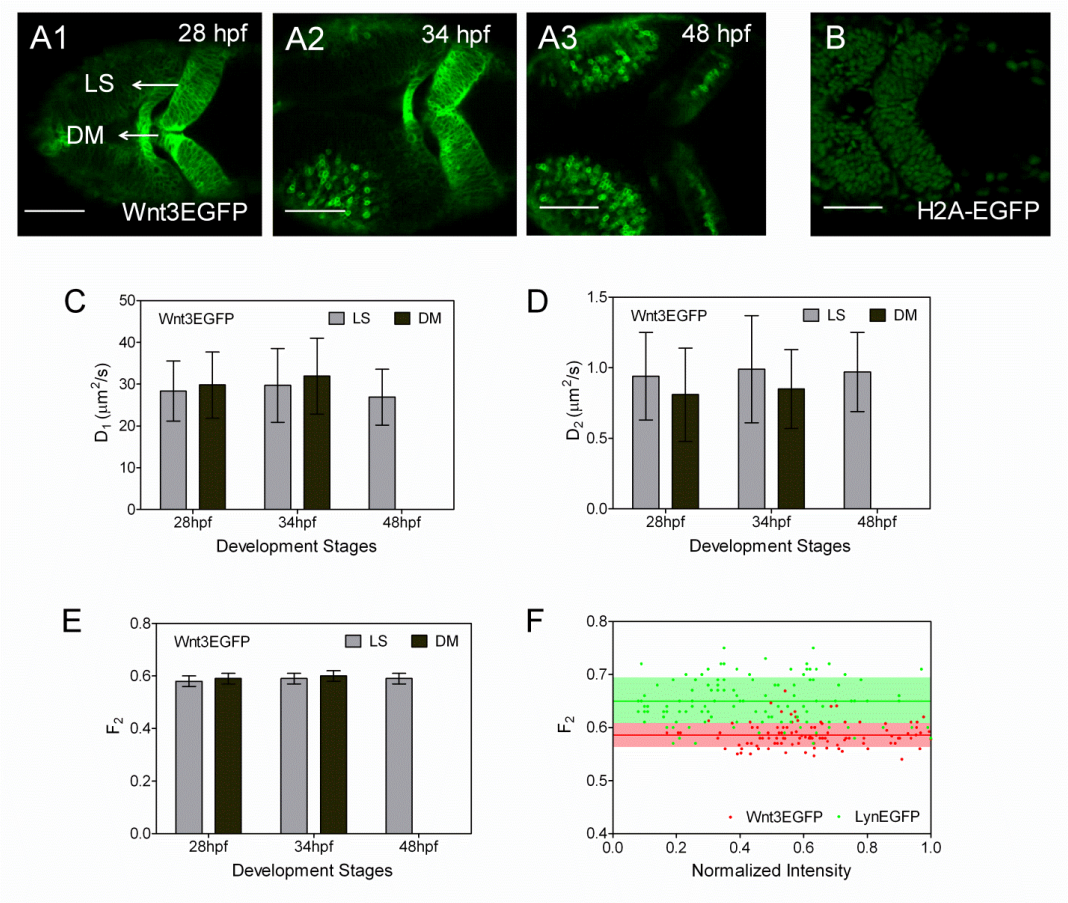


**Fig. S5. Wnt3EGFP fractions are in a stable equilibrium.** (A) Confocal images of zebrafish cerebellum (with optic tectum) expressing Wnt3EGFP at 28 hpf (A1), 34 hpf (A2), 48hpf (A3). The images show that Wnt3EGFP expression level differs in different regions of the cerebellum: lateral side (LS) and dorsal midline (DM). Images were taken in dorsal view. Scale bar, 200 μm. (B) Confocal image of zebrafish cerebellum (with optic tectum) expressing H2A-EGFP at 36 hpf shows that at this stage the nucleus occupies most of the inner space of the cell. Image was taken in dorsal view. Scale bar, 200 μm. (C, D and E) Diffusion coefficients ($D_1$, $D_2$) and fraction of slow moving component ($F_2$) extracted from fit at different development stages and regions in the cerebellum (LS and DM). The expression level in DM at 48 hpf was too low to be measured, therefore only data from LS were acquired. Data are mean ± SD. Light grey bar, LS. Dark grey bar, DM. (F) Fraction of slow moving component (F2) does not change with the protein expressing level, which is indicated by the normalized intensity count rate, for both Wnt3EGFP (red dot) and LynEGFP (green dot). Solid lines represent the mean and areas represent the SD respectively.

Abbreviations: Ce: cerebellum; BV: brain ventricle.

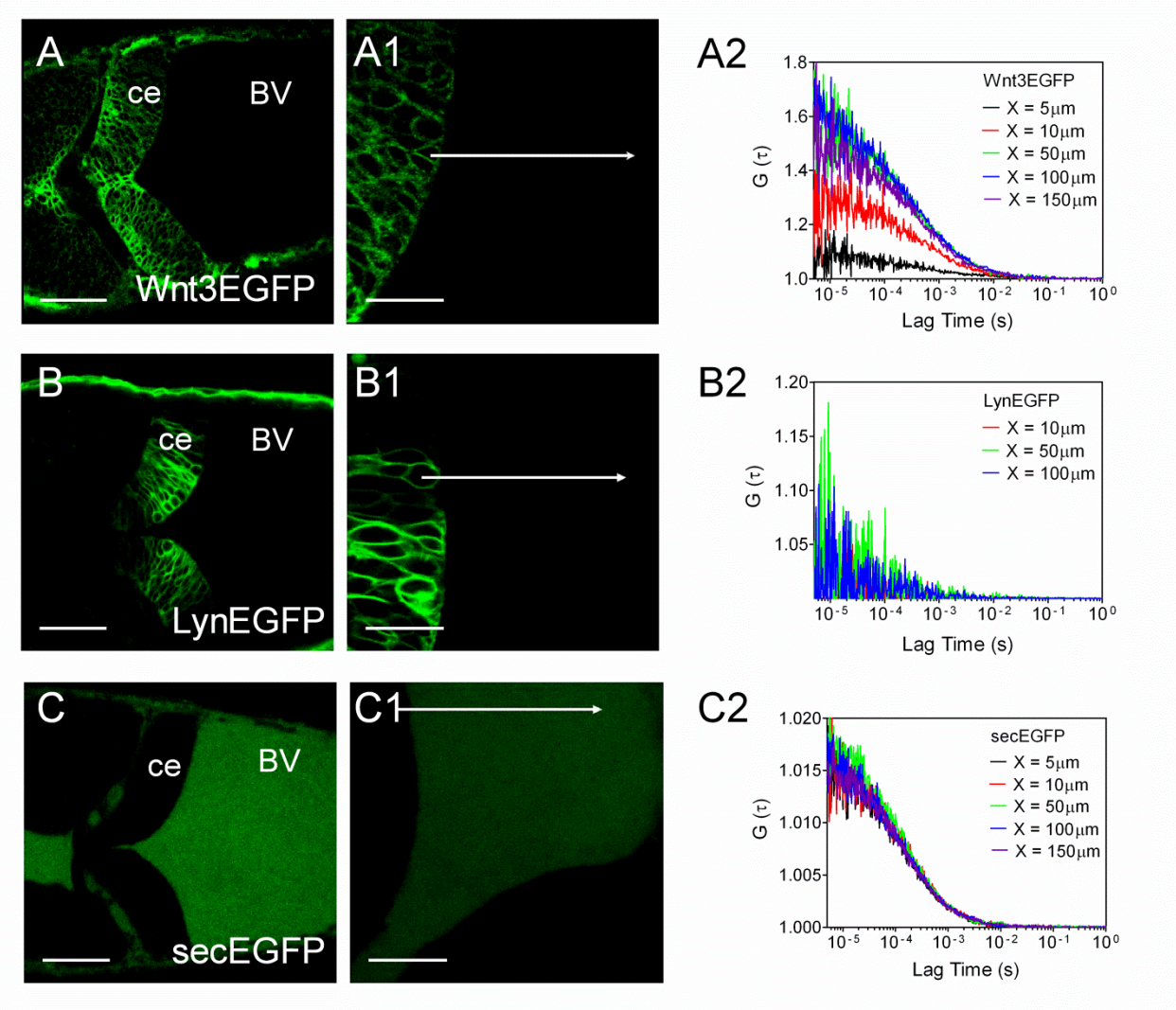


**Fig. S6. Secreted Wnt3EGFP in the brain ventricle.** (A, B, C) Confocal images of zebrafish cerebellum expressing Wnt3EGFP, LynEGFP and secEGFP at 34 hpf. Scale bar, 50 μm. Images were taken in dorsal view. A is the same as Fig. 6A. (A1, B1, C1) Three times zoom in of (A, B, C) with focus on the boundary of the cerebellum and brain ventricle. Scale bar, 20 μm. X-scanning was performed along the white arrow. Data were analysed using ImageJ. Results are shown in Fig. 6C in the main text. (A2, B2, C2) ACF curves of FCS measurements along the arrows at different distance from the cell boundary: 5μm (black); 10μm (red); 50μm (green); 100μm (blue); 150μm (purple). FCS data at 100 μm were normalized and plotted in Fig. 6D in the main text for comparison. Abbreviations: Ce: cerebellum; BV: brain ventricle.

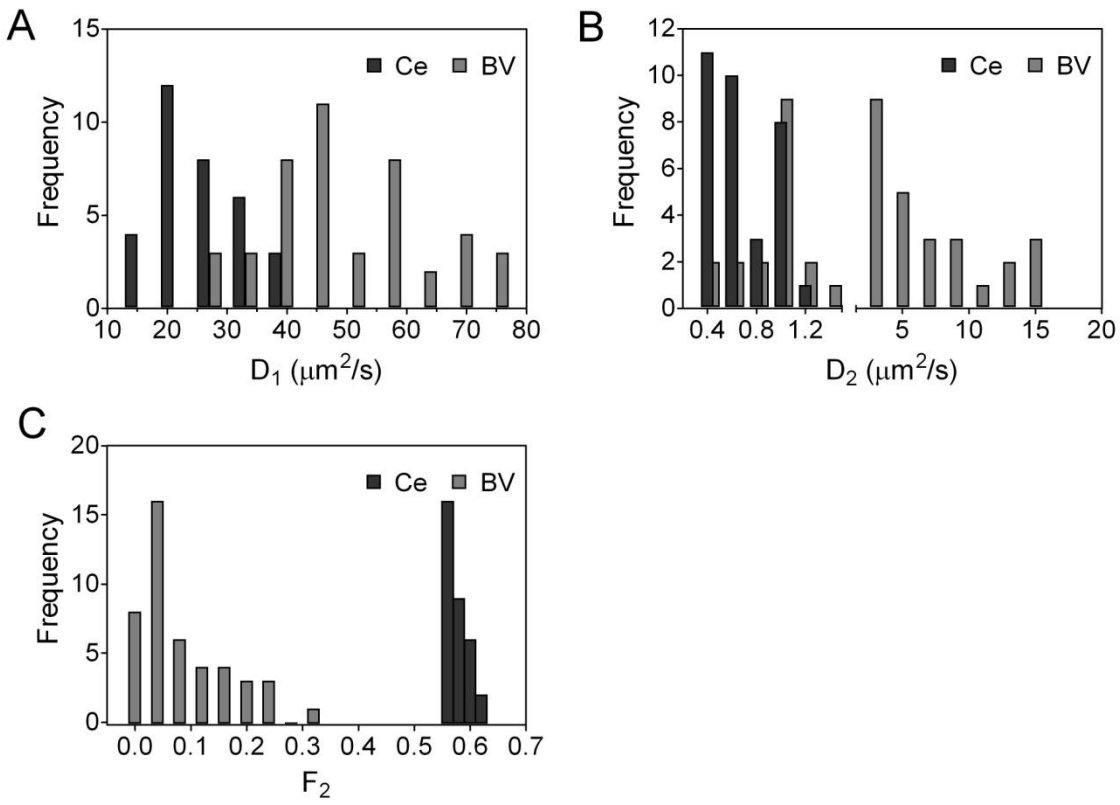


**Fig. S7. Heterogeneity of Wnt3EGFP in the brain ventricle.** Distribution of diffusion coefficients $D_1$ and $D_2$ (A and B) and fraction of slow moving component $F_2$ (C) in the cerebellum (dark grey bar) and in the brain ventricle (light grey bar), showing the mobility / size heterogeneity of the slow moving Wnt3EGFP in the brain ventricle. See also Table S2.

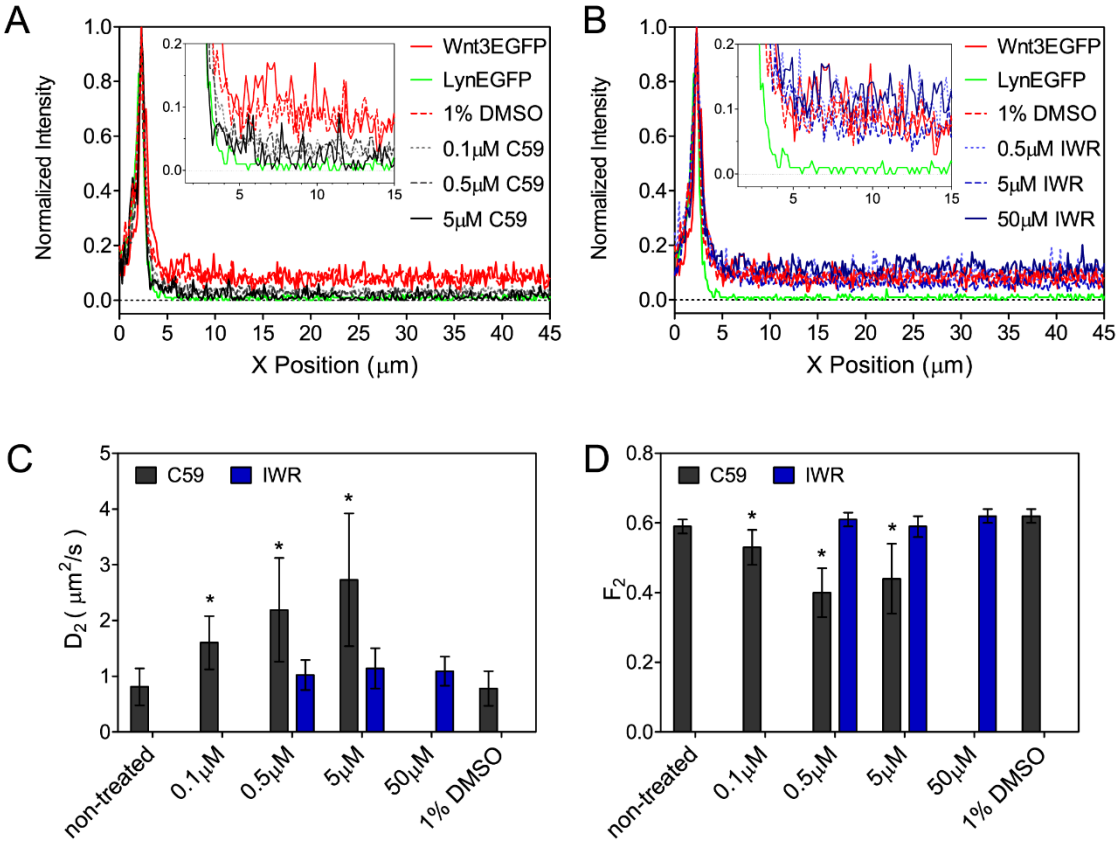


**Fig. S8. Comparison of Wnt3 secretion after C59 and IWR-1 treatments.** (A) Intensity line profiles of Wnt3EGFP and LynEGFP after treatment with C59. The line profiles extend from the plasma membrane of cerebellar cells flanking the 4$^{th}$ brain ventricle to ~40 µm into the BV. While the intensity within the BV does not change in the control with 1% DMSO, treatment with as low as 0.1 µM C59 leads to a marked reduction of Wnt3EGFP intensity in the BV. LynEGFP is not found in the BV. All curves are normalized to their maximum intensity at the plasma membrane. (B) Same as (A) but with IWR-1 treatment. Concentrations of IWR-1 between 0.5 – 50 µM have no effect on Wnt3EGFP secretion. (C) Comparison of membrane diffusion coefficient ($D_2$) of Wnt3EGFP under different treatment. Treatment with 0.1 – 5 µM C59 leads to significant increases in Wnt3EGFP diffusion on the membrane, presumably due to inhibition of lipid modification of Wnt3 by C59. A 1% DMSO control, as well as IWR-1 treatment (0.5 – 50 µM) had no effect. (D) Comparison of the membrane bound fraction ($F_2$) of Wnt3EGFP under different treatment. As in (C) only C59 shows any effects on the membrane bound fraction, overall decreasing $F_2$. The 1% DMSO control and IWR-1 (0.5 – 50 µM) had no effect.

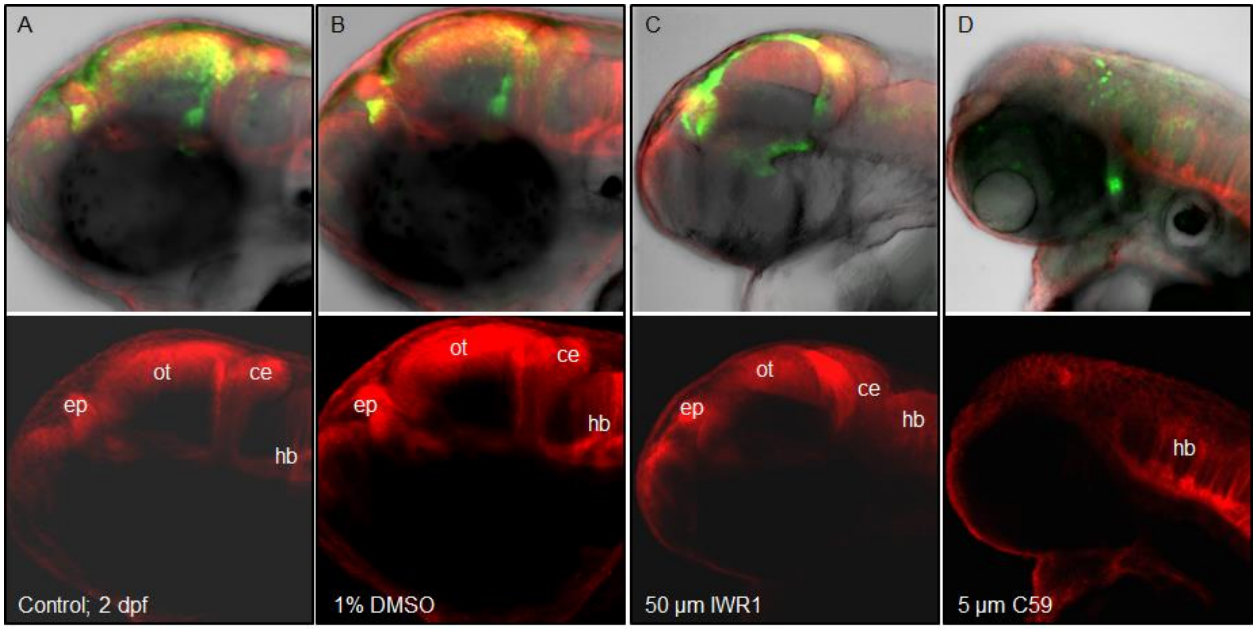


**Fig. S9. Effect of C59 Wnt inhibitor on brain patterning.** Exposure of Tg(*wnt3*:Wnt3EGFP)$^{F2}$ to C59 Wnt inhibitor suppresses Wnt3EGFP expression and interferes with brain patterning. Dorsal domains of the brain are highlighted by the expression of membrane tethered KillerRed in the epithalamus, optic tectum, cerebellum and hindbrain of Tg (memKR15-8). Double transgenic larvae were treated with 5 µM C59; 50 µM IWR-1 or 1% DMSO from 10 hpf to 48 hpf. Successful interference of Wnt function by C59 results in decreased Wnt3EGFP expression that correlated with defective brain patterning indicated by the absence of epithalamus (ep), optic tectum (ot) and cerebellum (ce) in C59 treated larvae (D).

**Table S1. FCS measurement on membrane Wnt3EGFP and LynEGFP at different development stages**

| Species | Development Stages (hpf) | $D_1$( $\mu m^2 s^{-1}$) | $D_2$ ($\mu m^2 s^{-1}$) | $F_2$ (%) | Total Embryo No. | Total Cell No. |
|---|---|---|---|---|---|---|
| Wnt3EGFP | 28 | 28.36 ± 7.17 | 0.94 ± 0.31 | 58 ± 2 | 5 | 24 |
| | *28 | 29.82 ± 7.88 | 0.81 ± 0.33 | 59 ± 2 | 4 | 30 |
| | 34 | 29.70 ± 8.81 | 0.99 ± 0.38 | 59 ± 2 | 5 | 22 |
| | *34 | 31.93 ± 9.06 | 0.85 ± 0.28 | 60 ± 2 | 6 | 28 |
| | 48 | 26.88 ± 6.68 | 0.97 ± 0.28 | 59 ± 2 | 5 | 26 |
| LynEGFP | 28 | 45.48 ± 10.10 | 3.04 ± 0.82 | 63 ± 4 | 6 | 35 |
| | 34 | 47.42 ± 13.19 | 3.46 ± 1.09 | 65 ± 3 | 6 | 35 |
| | 48 | 44.19 ± 16.39 | 2.43 ± 0.69 | 67 ± 5 | 5 | 33 |
| $EGFP^{F2}$ | 28 | 38.74 ± 8.54 | - | - | 3 | 30 |

Data are mean ± SD of number of cells measured. Measurements were performed in the lateral side (LS) region for comparison between Wnt3EGFP and LynEGFP. *Measurements performed in the dorsal midline (DM) region.

**Table S2. Protein mobility intracellularly, intercellularly and extracellularly**

| | 34hpf | D or $D_1$ ( $\mu m^2 s^{-1}$) | Embryo No. | Total Point No. |
|---|---|---|---|---|
| Ce | Wnt3EGFP | 29.70 ± 8.81 | 5 | 22 |
| | secEGFP | 53.97 ± 15.18 | 2 | 11 |
| | $EGFP^{F2}$ | 38.74 ± 8.54 | 3 | 30 |
| | LynEGFP | 47.42 ± 13.19 | 6 | 35 |
| BV | Wnt3EGFP | 53.62 ± 13.69 | 6 | 45 |
| | secEGFP | 125.82 ± 8.85 | 3 | 22 |

Data are mean ± SD of number of points measured. Ce: cerebellum; BV: brain ventricle.

**Table S3. Measurements on membrane for Wnt3EGFP and LynEGFP when treated by different Wnt inhibitors**

| Species | Conditions | $D_1$ ($\mu m^2 s^{-1}$) | $D_2$ ($\mu m^2 s^{-1}$) | $F_2$ (%) | Total Embryo No. | Total Cell No. |
|---|---|---|---|---|---|---|
| Wnt3EGFP | 5 μM C59 | 30.80 ± 7.38 | 2.73 ± 1.19 | 44 ± 10 | 4 | 29 |
| | 1% DMSO | 28.60 ± 5.01 | 0.78 ± 0.31 | 62 ± 2 | 1 | 8 |
| | 50 μM IWR1 | 33.79 ± 7.20 | 1.09 ± 0.26 | 62 ± 2 | 2 | 17 |
| LynEGFP | 5 μM C59 | 46.19 ± 11.34 | 2.86 ± 0.76 | 66 ± 4 | 3 | 24 |
| | 1% DMSO | 50.26 ± 11.31 | 3.28 ± 1.07 | 64 ± 4 | 2 | 11 |

Data are mean ± SD of number of cells measured.

**Table S4. Typical value of fitting parameters for calibration using Atto488**

| Fit Parameters | Fitting Value |
|---|---|
| N | 2.04 ± 0.08 |
| $\tau_D$ (μs) | 44 ± 3 |
| $\tau_{trip}$ (μs) | 6 ± 4 |
| $F_{trip}$ (%) | 16 ± 5 |
| K | 5.96 ± 0.93 |
| G(∞) | 0.9999 ± 0.0001 |

Data = mean ± SD

## Supplementary Materials and Methods

### Fluorescence Correlation Spectroscopy (FCS)

*Theory.* FCS extracts information from fluorescence signal fluctuations as fluorophores pass through a small observation volume (around $10^{-15}$ L). This small observation volume is created by focusing a laser to a diffraction limited volume. Processes generating the fluctuations could be, e.g., chemical reactions, rotational diffusion, translational diffusion or flow. The signals are then transformed to extract information embedded in the fluctuations by a temporal autocorrelation. The normalized autocorrelation function (ACF) can be written as:

$$G(\tau) = \frac{\langle F(t)F(t+\tau)\rangle}{\langle F(t)\rangle^2} \quad (1)$$

where F(t) is the fluorescence intensity at time t; ⟨ ⟩ denotes time average and τ is the lag time. Assuming a Gaussian laser profile, the theoretical ACF for 3D free diffusion of one species with a triplet state is given by (Aragón and Pecora, 1976):

$$G_{3D}(\tau) = \frac{1}{N}\left(1+\frac{\tau}{\tau_D}\right)^{-1}\left[1+\frac{1}{K^2}\left(\frac{\tau}{\tau_D}\right)\right]^{-1/2} f_{trip}(\tau) + G_\infty \quad (2)$$

where N is the average number of molecules in the observation volume; $\tau_D$ is the diffusion time the fluorophore taking to pass through the observation volume; $G_\infty$ is the convergence value of the ACF for long times with the expected value of 1;

$$K = \frac{\omega_z}{\omega_0} \quad (3)$$

$\omega_0$ and $\omega_z$ are the radial and axial distances where the excitation intensity reaches $1/e^2$ of its value at the center of the observation volume. K describes the shape of the observation volume;

$$f_{trip}(\tau) = \left(\frac{F_{trip}}{1-F_{trip}}\right) exp\left(-\frac{\tau}{\tau_{trip}}\right) + 1 \quad (4)$$

$F_{trip}$ is the fraction of the particles in the triplet state; $\tau_{trip}$ is the triplet state relaxation time. At higher laser intensities, a triplet state of the fluorophore can be populated. Typical triplet states have kinetics occurring on a timescale that is much faster than the diffusion time (Widengren et al., 1995; Widengren et al., 1999).

From Eq. 2, the amplitude of the ACF is:

$$G(0) = \frac{1}{N}\left(\frac{1}{1 - F_{trip}}\right) + G(\infty) \quad (5)$$

from where the average number of particles in the observation volume is given by:

$$N = \frac{1}{(G(0) - G(\infty))(1 \infty F_{trip})} \quad (6)$$

The size of the observation volume $V_{eff}$ can be estimated from a calibration using a dye with known diffusion coefficient by the following equations:

$$\tau_D = \frac{{\omega_0}^2}{4D} \quad (7)$$

$$V_{eff} = \pi^{3/2}{\omega_0}^2\omega_z = K\pi^{3/2}{\omega_0}^3 \quad (8)$$

Then, the absolute concentration ($C_i$) of a sample and its diffusion coefficient (D) can be determined by Eq. 9 and 10:

$$C_i = \frac{N}{N_A V_{eff}} \quad (9)$$

$$D = \frac{\tau_{D0} \times D_0}{\tau_D} \quad (10)$$

where $\tau_{D0}$ and $D_0$ are diffusion time and diffusion coefficient of the calibration dye.

When a fluorescently labelled molecule binds to a bigger unlabelled molecule, a change in the diffusion time should be detected using FCS. Similarly, when a fluorescently labelled molecule within a membrane, a longer diffusion time should be detected compared with a free moving molecule. In order to differentiate the changes in diffusion times in a FCS

experiment, the diffusion times of the two situations need to differ by at least 1.6 times (Meseth et al., 1999).

*Fitting Models* For the free diffusion of one fluorophore species passing through a 3D-Gaussian observation volume due to Brownian motion, such as measurements inside the cells and in the brain ventricle, the theoretical correlation function is given by Eq. 2. For membrane measurement, 2D or planar free diffusion models (Elson and Magde, 1974) are used:

$$G_{2D,1p}(\tau) = \frac{1}{N}\left(1+\frac{\tau}{\tau_D}\right)^{-1} f_{trip}(\tau) + G_\infty \quad (11)$$

In biological systems, processes under investigation sometimes consist of more than one diffusion components due to binding with bigger molecules or trafficking through the membrane. Multi-component models are used in these cases. The correlation functions for two components in 3D and 2D are described as:

$$G_{3D,2p}(\tau) = \frac{1}{N}\left(\begin{array}{l}(1-F_2)\left(1+\frac{\tau}{\tau_{D1}}\right)^{-1}\left(1+\frac{1}{K^2}\left(\frac{\tau}{\tau_{D1}}\right)\right)^{-\frac{1}{2}} \\ +F_2\left(1+\frac{\tau}{\tau_{D2}}\right)^{-1}\left(1+\frac{1}{K^2}\left(\frac{\tau}{\tau_{D2}}\right)\right)^{-\frac{1}{2}}\end{array}\right) f_{trip}(\tau) + G_\infty \quad (12)$$

$$G_{2D,2p}(\tau) = \frac{1}{N}\left[(1-F_2)\left(1+\frac{\tau}{\tau_{D1}}\right)^{-1} + F_2\left(1+\frac{\tau}{\tau_{D2}}\right)^{-1}\right] f_{trip}(\tau) + G_\infty \quad (13)$$

where $F_2$ is the fraction of the second component.

Eq.13 was chosen to fit the experimental data for Wnt3EGFP and LynEGFP in the cerebellum. Eq. 12 was chosen to fit the experimental data for Wnt3EGFP in the brain ventricle. Eq. 11 was chosen to fit the experimental data for EGFP of Tg(-4.0*wnt3*:EGFP)[F2] and secEGFP in the cerebellum and in the brain ventricle. The free parameters for a fit are N, $\tau_1$, $\tau_2$, $F_2$, $\tau_{trip}$, $F_{trip}$ and $G_\infty$. The parameter K describes the shape of the observation volume,

which is determined by the size of the laser focus and the pinhole. Therefore it is fixed from calibration of a known organic dye.

*Calibration.* Calibration measurement was routinely performed before the measurement using Atto488 (D = 400 $\mu m^2 s^{-1}$). A droplet of 60 µL of 5 nM sample solution was used. Laser power before the objective was 25 µW. Estimated observation volume $V_{eff}$ was 6.60 □ $10^{-16}$ L. FCS data was fitted with Eq.2, typical results of all fitting parameters are given in Table S4.

*Experiments.* Embryos at the stage of interest (24 - 72 hpf) were dechorionated and then anaesthetized by Tricaine (ethyl m-aminoboenzoate, Sigma). The treated embryos were mounted in 1% low melting temperature agarose (Invitrogen) in a No. 1.5 coverglass bottom Petri dish (MatTek, USA) for subsequent measurements. Different orientations (eg. dorsal view or lateral view) of the embryos can be adjusted with needle. Laser power measured before the objective was 15 µW. The acquisition time for a membrane measurement was 15 s and a measurement in the brain ventricle 20s. The measurements were performed at room temperature.